

Berry phase manipulation in ultrathin SrRuO₃ films

Liang Wu,^{1,*} Fangdi Wen,^{1,†} Yixing Fu,^{1,2} Justin H. Wilson,^{1,2} Xiaoran Liu,¹ Yujun Zhang,³ Denis M. Vasiukov,¹ Mikhail S. Kareev,¹ J. H. Pixley,^{1,2} and Jak Chakhalian¹

¹*Department of Physics and Astronomy, Rutgers University, Piscataway, NJ 08854, USA*

²*Center for Materials Theory, Rutgers University, Piscataway, NJ 08854, USA*

³*Institute for Solid State Physics, University of Tokyo, 5-1-5 Kashiwanoha, Chiba 277-8581, Japan*

(Dated: July 18, 2019)

A notion of the Berry phase is a powerful means to unravel the non-trivial role of topology in various novel phenomena observed in chiral magnetic materials and structures. A celebrated example is the intrinsic anomalous Hall effect (AHE) driven by the non-vanishing Berry phase in the momentum space. As the AHE is highly dependent on details of the band structure near the Fermi edge, the Berry phase and AHE can be altered in thin films whose chemical potential is tunable by dimensionality and disorder. Here, we demonstrate that in ultrathin SrRuO₃ films the Berry phase can be effectively manipulated by the effects of disorder on the intrinsic Berry phase contribution to the AHE, which is corroborated by our numerically exact calculations. In addition, our findings provide ample experimental evidence for the superficial nature of the topological Hall effect attribution to the protected spin texture and instead lend strong support to the multi-channel AHE scenario in ultrathin SrRuO₃.

During the last decade, a search for topologically non-trivial modalities in both real and momentum space has become a dominant driver in condensed matter physics [1–6]. A metallic magnet entwined with a non-collinear spin texture like skyrmions, domain walls, or helical order can demonstrate interesting phenomena due to the interaction of conduction carriers with the localized spins [5–8]. Microscopically, such non-trivial magneto-transport response stems from the emergent electromagnetic fields (EEMFs) linked to the finite Berry phase accumulation. From the experimental standpoint, the challenge is to devise clear signatures of the EEMFs linked to the topologically protected spin texture with a non-zero winding number or skyrmions. Recently, it has been realized that such skyrmionic contribution can be revealed as the extra features to the transverse Hall resistivity ρ_{xy} arising from a fictitious Lorentz force [6, 9]. This contribution to the anomalous Hall effect (AHE) is collectively known as the topological Hall effect or THE. Because of the relative simplicity of the detection method, THE has quickly become a popular means to interrogate bulk, thin films and hetero-junctions of various materials for the presence of skyrmionic matter [10–23].

The criterion for the observation of THE is the extra bumps/dips along with the AHE, however, which is only valid for *homogenous materials with a single conduction channel* [24–26]. Moreover, the effects of disorder which are always present in real materials, can drastically alter the Berry phase and AHE, and yet are typically removed from the consideration. In this work, we interrogate the validity of the THE for a prototypical magnet SrRuO₃ (SRO) grown in the ultrathin form to amplify the effects of confinement, and magnetic and structural inhomogeneity on the Berry phase and AHE. As the Berry

phase and AHE behavior in SRO are highly dependent on details of the band structure near the Fermi surface, we demonstrate how both entities can be effectively manipulated in the ultrathin limit of SRO. Using a phenomenological model that displays the THE-like Hall signal, we theoretically capture the experimentally observed tunability of the AHE with film-thickness, disorder, and temperature. More specifically, by including the effect of inhomogeneity to analyze the experimental data in the form of a two-channel AHE with opposite signs, we are able reproduce both the overall transverse Hall effect and the universal scaling behavior between AHE conductivity σ_{AHE} and longitudinal conductivity σ_{xx} without resorting to THE.

In this work we focus on SrRuO₃ (SRO), an exemplary ferromagnetic metal with perovskite structure with a Curie temperature $T_c \approx 150\text{K}$ [27–29]. The investigation of the Hall effect in SRO not only played an important role in separating the intrinsic nature of AHE from extrinsic contributions [30–33], but also accelerated the research on THE and skyrmions [20–23]. However, the AHE in SRO also exhibits a complex non-monotonous dependence on thickness and temperature [20, 21, 30, 34], which in turn demands scrutiny of the experimental results.

To investigate the temperature dependence of the AHE as a function of confinement, we have acquired a series of temperature (T)-dependent resistivity curves shown in Fig. 1a. In addition to the pristine samples we have developed a protocol to introduce controlled disorder by time-exposing the as-grown samples (labeled as series A samples of 4 u.c. and 5 u.c., which is short for 4A and 5A) to ambient conditions (labeled as series B samples, 4B and 5B). As seen, all films display a common feature, namely, a metallic state at high temperature and a small kink at around 100 K indicating the paramagnetic to ferromagnetic phase transition, which is lower than that of the bulk [20, 21, 35]. In addition, a characteristic up-

* lw590@physics.rutgers.edu

† fw113@physics.rutgers.edu

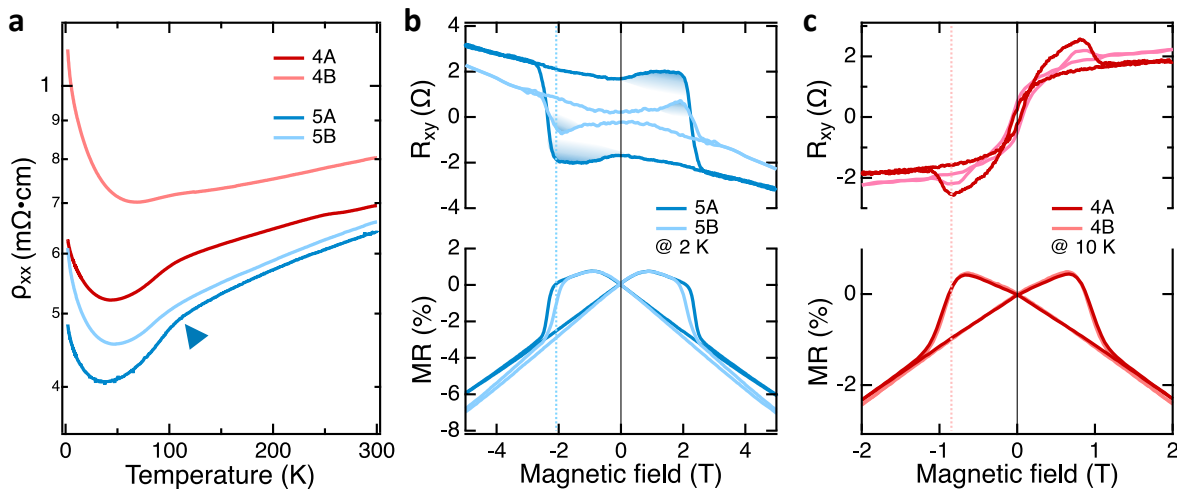


Figure 1. Longitudinal and transverse transport results of ultrathin SRO films. **a**, temperature dependence of resistivity ρ_{xx} , red and blue curves indicate the sample with as-grown (A) and air-exposed (B) conditions, respectively. **b-c**, MR and Hall measurements of 5 u.c. and 4 u.c. samples at 2 and 10 K, respectively. Note, the shaded areas are attributed to the THE-like Hall contribution.

turn appears below 40 K, which is due to Anderson weak localization in the ultrathin limit. Further, as immediately seen in Figs 1b and 1c for both 4B and 5B samples the R-T curves still retain the characteristic shape of the as-grown samples 4A and 5A, albeit with larger resistivity and steeper upturn at the low temperature characteristic of enhanced disorder. Interestingly, the magnetoresistance (MR) measurements, however, show only a negligible difference between the A and B series samples (see Fig. 1b, c) implying that disorder barely impacts ferromagnetism in SRO. With this understanding, we conduct T-dependent Hall measurements to investigate the thickness- and disorder-dependent AHE at different temperatures. Figures 1b and 1c show the representative low-temperature Hall resistance data. Following the convention, a magnitude of anomalous Hall resistance is extrapolated from the high-field linear part of the data, whose sign defines the sign of AHE, namely, the AHE in 4A (or 5A) is referred to positive (or negative). This attribution is consistent with the previous reports [20, 21, 34]. A direct inspection of Fig. 1b and 1c, however, reveals an unexpected result that the Hall data undergo a strong change for the B-series samples.

Next we apply the data analysis which is conventionally used to extract THE and separate various contributions to the Hall effect in SRO. Under the assumption of an idealized sample and in the presence of skyrmions, the Hall resistance can be decomposed as $R_{xy} = R_{\text{OHE}} + R_{\text{AHE}} + R_{\text{THE}}$ [20, 21, 34], where the R_{OHE} stands for ordinary Hall effect (OHE). Alternatively, the THE-like Hall resistance can also be decomposed as $R_{xy} = R_{\text{OHE}} + R_{\text{AHE}}^+ + R_{\text{AHE}}^-$, where the last two terms denote a positive and negative sign AHEs of the two-channel AHE [24, 26]. In the following discussions,

all OHE has been subtracted by fitting the high field linear slope. Given that complex oxide perovskites in the film form often exhibit intrinsic propensity to defects and layer non-uniformity during the step-flow growth, we demonstrate that the minimal two-channel AHE without THE can successfully capture all the AHE features across the whole temperature range. First, we remind the reader that a thickness variation of at least 1 u.c. practically always exists in a real film since step edges on the surface of an SRO film cannot ideally replicate those of the substrate after the growth. This intrinsic thickness non-uniformity, though often ignored in thicker films, upon approaching the ultrathin limit can strongly alter the Hall transport. Experimentally, the thickness variation in SRO was recently observed by magnetic force microscopy [21]. In addition, the two-step transitions found in magnetic hysteresis loops [35, 36] and MR shown in Fig. 1b lend strong support for the thickness variation of the nominal SRO thickness.

As seen in Fig. 2, remarkably, for the 4A film the sign of AHE is *opposite* to that of the 5A sample below the crossover temperature around 90K [20, 21, 34]. Given the above discussed intrinsic variation of the thickness, we are able to successfully reproduce the total AHE of the nominal 5 u.c. sample as the sum of the positive (4 u.c.) and negative AHEs (5 u.c.) originating from the thickness variation throughout the SRO film, without the 'superficial' THE feature. This result strongly suggests that the thickness-dependent AHE sign reversal and disorder are the most probable underlying physical mechanisms for the extra features of the AHE. Next, we quantify the individual AHE contributions within the two-channel model in 5 u.c. SRO (4 u.c. SRO data are given in Supplementary Fig. S2) to elucidate

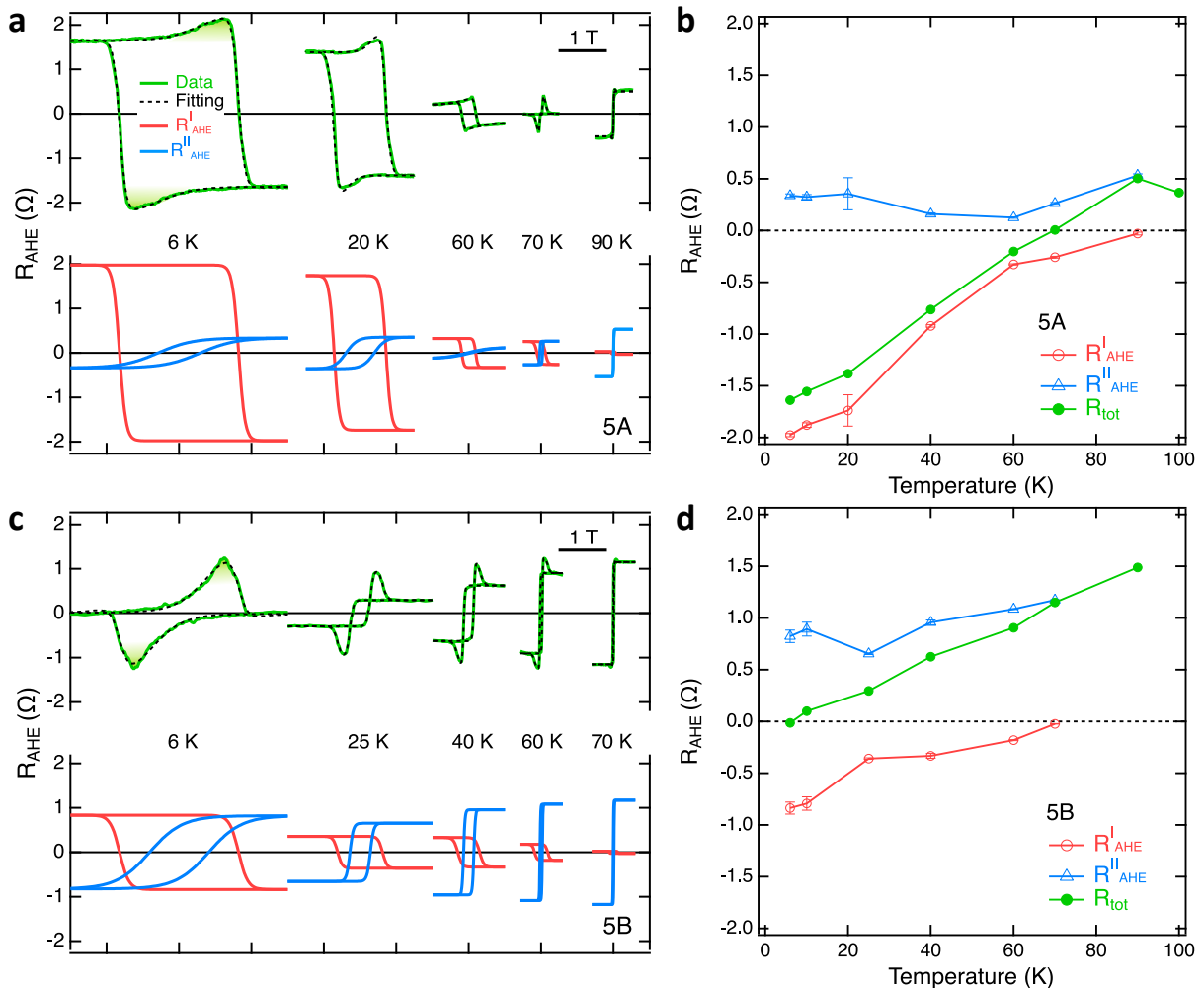


Figure 2. Disentanglement of two-channel AHE in 5 u.c. SRO. **a**, Upper panel, the experimental AHE data and their fitting results of 5A, lower panel, the separation of the two AHE channels of 5A. **b**, Temperature dependent total and two-channel AHE. **c-d**, same data treatment for 5B. When both two channels are positive and have similar H_c it is infeasible to separate those contributions.

the role of disorder and dimensionality on the AHE as: $R_{\text{AHE}}^{\text{tot}} = R_{\text{AHE}}^{\text{I}} \tanh(\omega_{\text{I}}(H - H_c^{\text{I}})) + R_{\text{AHE}}^{\text{II}} \tanh(\omega_{\text{II}}(H - H_c^{\text{II}}))$, where H_c and ω denote coercive field and slope related parameter at H_c for each channel. Figure 2a (top panel) shows the experimental AHE data and results of the fit. A direct inspection of Fig. 2 confirm that the fitting curves are indeed in excellent agreement with the experimental data and require no additional THE-like contribution. Another backing for the proposed two-channel model is found in the T-dependence of the total and the two-channel AHE shown in Fig. 2. As seen, of the data that at 90 K for the sample 5A the THE-like features completely disappear. For the disorder induced sample 5B, however, the total AHE remain positive through the whole temperature range. This comparison implies that the disorder indeed makes a strong positive contribution to the Berry phase part of the AHE. The physical mechanism of how disorder interacts with

the Berry phase will be discussed in detail below.

Further, to verify the validity of the two-channel AHE model, we apply the scaling relation between the magnitude of anomalous Hall conductivity $|\sigma_{\text{AHE}}|$ vs. longitudinal conductivity σ_{xx} . This universal scaling relation broadly subdivides all materials systems into three regimes [25, 37–39]. For ultrathin SRO, $\sigma_{xx} \leq 10^4 \Omega^{-1}\text{cm}^{-1}$ implies that the material is a subject to disorder that smears the contribution from intrinsic Berry phase driven AHE, resulting in the scaling relation for $\sigma_{\text{AHE}} \propto (\sigma_{xx})^{1.6}$.

Next, we map our data on to the universal scaling curve to verify the THE and two-channel AHE scenarios. Here, we note that in the THE scenario, the extra THE contribution to the Hall measurements vanish at a high magnetic field due to the spin texture alignment by a sufficiently large magnetic field [20, 21, 34]. As a result, if SRO contains a real THE contribution,

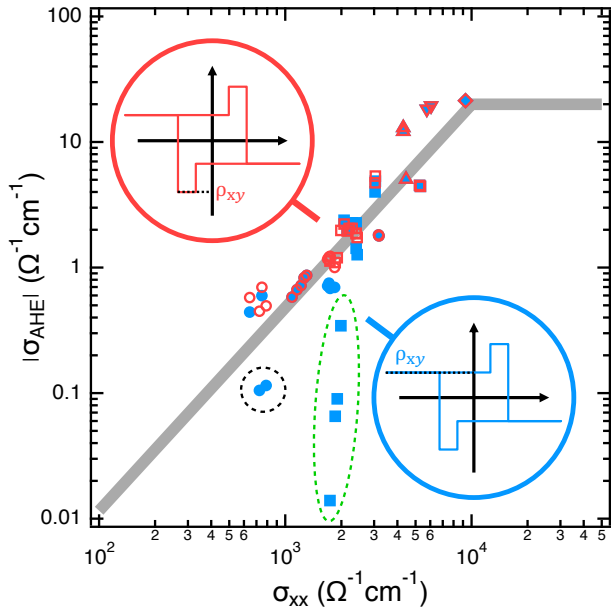


Figure 3. Comparison of the scaling relation. Blue filled and red open symbols are scaling relation derived in THE scenario and two-channel AHE scenario, respectively. The black and green dash circles indicate the large deviation from the universal scaling relation of BaTiO₃-capped 4 u.c. SRO [21] and 5B, where large THE-like Hall signal appears simultaneously.

the data extracted from AHE in the high magnetic field regime still should follow the universal scaling relation. Figure 3 shows the experimental results based on both THE and our two-channel AHE scenarios (see the Supplementary, section 3) along with the summary of previously published SRO data [20, 21]. As immediately seen, the THE scenario sharply diverges from the universal scaling, whereas our scaling data derived from the two-channel scenario show excellent consistency with the universal scaling relation.

Finally, we discuss the physical mechanism of the observed thickness, disorder, and temperature dependence on the AHE sign reversal in ultrathin SRO films (Fig. 1) with numerically exact calculations on a phenomenological lattice model [30]. In bulk three-dimensional models, it is known that temperature can induce a sign reversal in the AHE [30]. Here, we demonstrate that in disordered thin film samples varying the thickness and or the strength of disorder can similarly induce a reversal of sign in the AHE.

The model we use is a spin-polarized tight-binding model with d_{xz} and d_{yz} orbitals (originating from the t_{2g} orbitals) from Ref.[30] that is known to host an AHE and apply it to disordered thin films. The model is on a square lattice with spin-orbit coupling, with a finite magnetization, and with orbitals that induce nearest and next-nearest neighbor hoppings (with strength t_1 and t_2

respectively) on each individual u.c. while each u.c. is tunnel-coupled (with strength t_1). We consider slab sizes of $L_x = L_y = L = 233$ and vary the number of u.c. $L_z = 1 - 7$ with open boundary conditions in the z -direction and periodic in the x - and y -direction. While the features we see appear generic over different parameters and different types of disorder [Supplementary Section 4], we focus here on on-site potential disorder with strength W . Using the kernel polynomial method [40] we compute the full conductivity tensor [41] and hence the resistivity. The exact model, details of the calculation, and a broader consideration of the parameters and finite size can be found in Supplementary Section 4.

The numerical results are presented in Fig. 4 for the Hall resistivity ρ_{xy} . In the theory section, the only contribution for ρ_{xy} is ρ_{AHE} . At a particular disorder strength that we label W^* , the sign of the AHE changes. We precisely define this as the point at $E_F = 0$ when the slope of ρ_{xy} changes signs. Our results clearly demonstrate that the sign of ρ_{xy} changes due to varying the strength of disorder (Fig. 4a), the number of layers (Fig. 4b), and the temperature (Fig. 4c). In Fig. 4d we fix the temperature and find W^* as a function of number of u.c.. If we contrast the change in the AHE between disorder and temperature, we notice that increasing disorder is providing an enhancement of ρ_{xy} near $E_F \approx 0.5t_1$ in Fig. 4a whereas increasing temperature is tending to suppress this feature Fig. 4c. In the experiment, thinner films have larger disorder, and thus the experiment is taking a cut across the W^* boundary in Fig. 4d. As we cannot disentangle these two effects, the theoretical calculations demonstrate that the experimental results exhibit a sign reversal in the AHE due to varying both the number of layers and the strength of disorder.

In this few u.c. model, the density of states (Supplementary Section 6) shows that each u.c. creates a pair of van Hove peaks, with an offset due to hopping in the z -direction. Using the van Hove peaks as a guide, the distance between neighboring peaks near zero energy, denoted as ΔE , reduces with increased number of u.c. and Fig. 4d shows that this trend is correlated with W^* . As the number of u.c. increases the sign reversal in ρ_{xy} occurs when the disorder strength smears the two van Hove peaks closest to $E_F = 0$ into one. This is a signal of the general phenomena: due to the nonuniform distribution of Berry curvature in the bands, the inclusion of terms which sample states with different Berry curvature (e.g. temperature, disorder, and thickness) can significantly alter the AHE, even changing its sign.

In conclusion, the presented results unveil the unexpected thickness-dependent sign reversal in the AHE signal at the ultrathin limit. Such extreme sensitivity stems from the effects of disorder of the intrinsic Berry phase contribution of the AHE as confirmed by numerically exact calculations with the kernel polynomial method on a model that hosts the AHE. In addition, our findings provide strong experimental evidence for the super-ficial nature of the THE attribution to topologically pro-

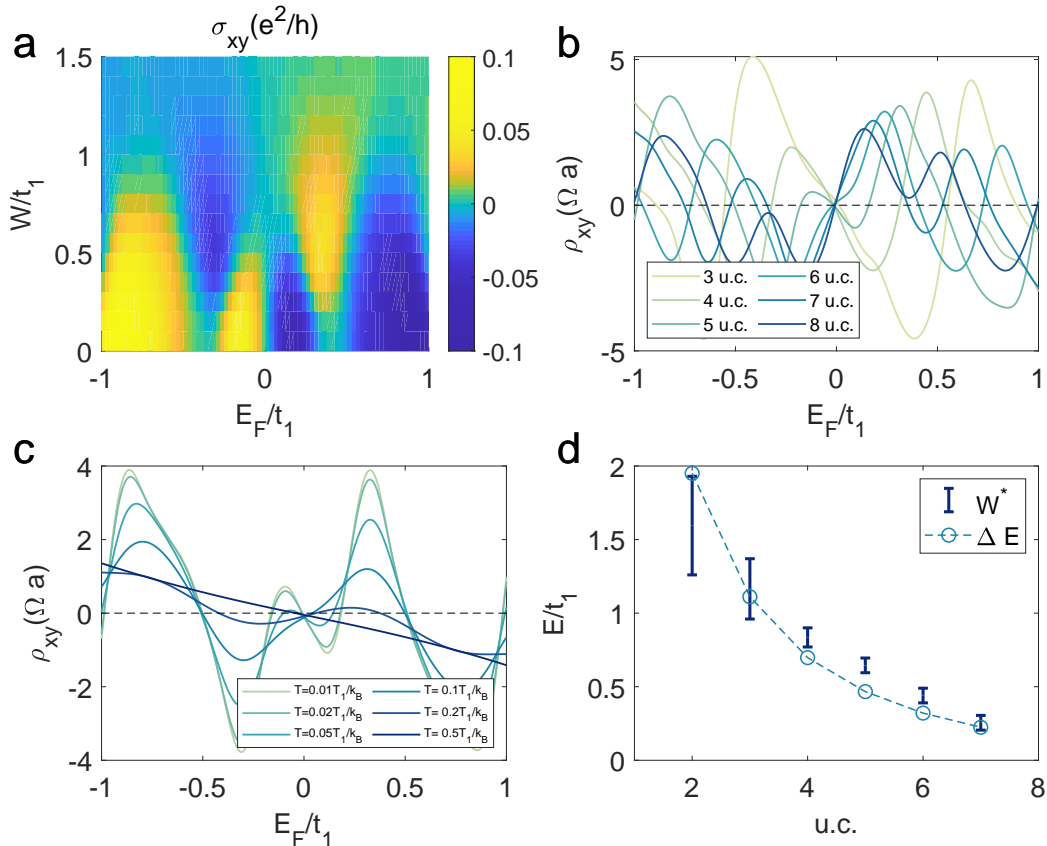


Figure 4. **a**, Anomalous Hall conductivity σ_{AHE} vs disorder strength W and Fermi energy E_F . **b-c**, Anomalous Hall resistivity ρ_{AHE} versus E_F for different **b** number of u.c. and **c**, temperatures. Notice that for each case there is a particular value of the changing variable where the AHE changes sign. In the case of disorder strength, we call this value W^* . For **a** and **b** the temperature is held at $T = 0.025t_1/k_B$, **b** and **c** hold the disorder constant at $W = 0.5t_1$, and **a** and **c** are for 5 u.c.. In **d** we show the relation between W^* and number of u.c. as well as the distance between the van-Hove peaks nearest to $E_F = 0$ in the disorder free limit for $T = 0.025t_1/k_B$. These quantities are correlated due to how they are related to the Berry curvature distribution within the bands.

tected spin texture and instead lend strong support to the two-channel AHE in SRO. The proposed multi-channel magneto-transport framework can be readily extended

to many other ultrathin chiral magnets with spin-order where disorder, and the effects of surface and interface are critically important.

-
- [1] M. Z. Hasan and C. L. Kane. Topological insulators. *Rev. Mod. Phys.*, 82:3045–3067, 2010.
- [2] X. L. Qi and S. C. Zhang. Topological insulators and superconductors. *Rev. Mod. Phys.*, 83:1057–1110, 2011.
- [3] N. P. Armitage, E. J. Mele, and A. Vishwanath. Weyl and Dirac semimetals in three-dimensional solids. *Rev. Mod. Phys.*, 90:015001, 2018.
- [4] A. Bansil, H. Lin, and T. Das. Topological band theory. *Rev. Mod. Phys.*, 88:021004, 2016.
- [5] N. Nagaosa and Y. Tokura. Topological properties and dynamics of magnetic skyrmions. *Nat. Nanotechnol.*, 8(12):899–911, 2013.
- [6] Y. Shiomi. *Anomalous and topological Hall effects in itinerant magnets*. Springer Theses, 2013.
- [7] S. Emori, U. Bauer, S. M. Ahn, E. Martinez, and G. S. D. Beach. Current-driven dynamics of chiral ferromagnetic domain walls. *Nat. Mat.*, 12:611, 2013.
- [8] S. Chakraverty, T. Matsuda, H. Wadati, J. Okamoto, Y. Yamasaki, H. Nakao, Y. Murakami, S. Ishiwata, M. Kawasaki, Y. Taguchi, Y. Tokura, and H. Y. Hwang. Multiple helimagnetic phases and topological Hall effect in epitaxial thin films of pristine and Co-doped SrFeO₃. *Phys. Rev. B*, 88:220405, 2013.
- [9] S. Zhang. *Chiral and topological nature of magnetic skyrmions*. Springer Theses, 2018.
- [10] A. Neubauer, C. Pfleiderer, B. Binz, A. Rosch, R. Ritz, P. G. Niklowitz, and P. Boni. Topological Hall effect in the A phase of MnSi. *Phys. Rev. Lett.*, 102(18):186602,

- 2009.
- [11] M. Lee, W. Kang, Y. Onose, Y. Tokura, and N. P. Ong. Unusual Hall effect anomaly in MnSi under pressure. *Phys. Rev. Lett.*, 102:186601, 2009.
- [12] A. Soumyanarayanan, M. Raju, A. L. Gonzalez Oyarce, A. K. C. Tan, M.-Y. Im, A. P. Petrovi, P. Ho, K. H. Khoo, M. Tran, C. K. Gan, F. Ernult, and C. Panagopoulos. Tunable room-temperature magnetic skyrmions in Ir/Fe/Co/Pt multilayers. *Nat. Mat.*, 16:898, 2017.
- [13] T. Schulz, R. Ritz, A. Bauer, M. Halder, M. Wagner, C. Franz, C. Pfleiderer, K. Everschor, M. Garst, and A. Rosch. Emergent electrodynamics of skyrmions in a chiral magnet. *Nat. Phys.*, 8:301, 2012.
- [14] Y. Ohuchi, Y. Kozuka, M. Uchida, K. Ueno, A. Tsukazaki, and M. Kawasaki. Topological Hall effect in thin films of the Heisenberg ferromagnet EuO. *Phys. Rev. B*, 91:245115, 2015.
- [15] M. Nakamura, D. Morikawa, X. Yu, F. Kagawa, T. Arima, Y. Tokura, and M. Kawasaki. Emergence of topological Hall effect in half-metallic manganite thin films by tuning perpendicular magnetic anisotropy. *J. Phys. Soc. Jpn.*, 87(7):074704, 2018.
- [16] Y. Li, N. Kanazawa, X. Z. Yu, A. Tsukazaki, M. Kawasaki, M. Ichikawa, X. F. Jin, F. Kagawa, and Y. Tokura. Robust formation of skyrmions and topological Hall effect anomaly in epitaxial thin films of MnSi. *Phys. Rev. Lett.*, 110:117202, 2013.
- [17] B. M. Ludbrook, G. Dubuis, A. H. Puichaud, B. J. Ruck, and S. Granville. Nucleation and annihilation of skyrmions in Mn₂CoAl observed through the topological Hall effect. *Sci. Rep.*, 7(1):13620, 2017.
- [18] C. Liu, Y. Zang, W. Ruan, Y. Gong, K. He, X. Ma, Q. K. Xue, and Y. Wang. Dimensional crossover-induced topological Hall effect in a magnetic topological insulator. *Phys. Rev. Lett.*, 119:176809, 2017.
- [19] Q. L. He, G. Yin, A. J. Grutter, L. Pan, X. Che, G. Yu, D. A. Gilbert, S. M. Disseler, Y. Liu, P. Shafer, B. Zhang, Y. Wu, B. J. Kirby, E. Arenholz, R. K. Lake, X. Han, and K. L. Wang. Exchange-biasing topological charges by antiferromagnetism. *Nat. Commun.*, 9(1):2767, 2018.
- [20] J. Matsuno, N. Ogawa, K. Yasuda, F. Kagawa, W. Koshibae, N. Nagaosa, Y. Tokura, and M. Kawasaki. Interface-driven topological Hall effect in SrRuO₃-SrIrO₃ bilayer. *Sci. Adv.*, 2(7):e1600304, 2016.
- [21] L. Wang, Q. Feng, Y. Kim, R. Kim, K. H. Lee, S. D. Pollard, Y. J. Shin, H. Zhou, W. Peng, D. Lee, W. Meng, H. Yang, J. H. Han, M. Kim, Q. Lu, and T. W. Noh. Ferroelectrically tunable magnetic skyrmions in ultrathin oxide heterostructures. *Nat. Mater.*, 17(12):1087–1094, 2018.
- [22] Q. Qin, L. Liu, W. Lin, X. Shu, Q. Xie, Z. Lim, C. Li, S. He, G. M. Chow, and J. Chen. Emergence of topological Hall effect in a SrRuO₃ single layer. *Adv. Mater.*, 31(8):e1807008, 2019.
- [23] K. Y. Meng, A. S. Ahmed, M. Bacani, A. O. Mandru, X. Zhao, N. Bagues, B. D. Esser, J. Flores, D. W. McComb, H. J. Hug, and F. Yang. Observation of nanoscale skyrmions in SrIrO₃/SrRuO₃ bilayers. *Nano Lett.*, 19(5):3169–3175, 2019.
- [24] D. Kan, T. Moriyama, K. Kobayashi, and Y. Shimakawa. Alternative to the topological interpretation of the transverse resistivity anomalies in SrRuO₃. *Phys. Rev. B*, 98(18):180408, 2018.
- [25] K. S. Takahashi, H. Ishizuka, T. Murata, Q. Y. Wang, Y. Tokura, N. Nagaosa, and M. Kawasaki. Anomalous Hall effect derived from multiple Weyl nodes in high-mobility EuTiO₃ films. *Sci. Adv.*, 4(7):eaar7880, 2018.
- [26] D. J. Groenendijk, C. Autieri, T. C. van Thiel, W. Brzezicki, N. Gauquelin, P. Barone, K. H. W. van den Bos, S. van Aert, J. Verbeeck, A. Filippetti, S. Picozzi, M. Cuoco, and A. D. Caviglia. Berry phase engineering at oxide interfaces. *Preprint at <https://arxiv.org/abs/1810.05619>*, 2018.
- [27] C. B. Eom, R. J. Cava, R. M. Fleming, J. M. Phillips, R. B. Vandover, J. H. Marshall, J. W. Hsu, J. J. Krajewski, and Jr. Peck, W. F. Single-crystal epitaxial thin films of the isotropic metallic oxides Sr_{1-x}Ca_xRuO₃ (0 ≤ x ≤ 1). *Science*, 258(5089):1766–9, 1992.
- [28] P. B. Allen, H. Berger, O. Chauvet, L. Forro, T. Jarlborg, A. Junod, B. Revaz, and G. Santi. Transport properties, thermodynamic properties, and electronic structure of SrRuO₃. *Phys. Rev. B*, 53:4393–4398, 1996.
- [29] G. Koster, L. Klein, W. Siemons, G. Rijnders, J. S. Dodge, C. B. Eom, D. H. A. Blank, and M. R. Beasley. Structure, physical properties, and applications of SrRuO₃ thin films. *Rev. Mod. Phys.*, 84(1):253–298, 2012.
- [30] Z. Fang, N. Nagaosa, K. S. Takahashi, A. Asamitsu, R. Mathieu, T. Ogasawara, H. Yamada, M. Kawasaki, Y. Tokura, and K. Terakura. The anomalous Hall effect and magnetic monopoles in momentum space. *Science*, 302(5642):92–5, 2003.
- [31] R. Mathieu, A. Asamitsu, H. Yamada, K. S. Takahashi, M. Kawasaki, Z. Fang, N. Nagaosa, and Y. Tokura. Scaling of the anomalous Hall effect in Sr_{1-x}Ca_xRuO₃. *Phys. Rev. Lett.*, 93(1):016602, 2004.
- [32] Y. Chen, D. L. Bergman, and A. A. Burkov. Weyl fermions and the anomalous Hall effect in metallic ferromagnets. *Phys. Rev. B*, 88:125110, 2013.
- [33] Y. Kats, I. Genish, L. Klein, J. W. Reiner, and M. R. Beasley. Testing the Berry phase model for extraordinary Hall effect in SrRuO₃. *Phys. Rev. B*, 70:180407, 2004.
- [34] B. Sohn, B. Kim, S. Y. Park, H. Y. Choi, J. Y. Moon, T. Choi, Y. J. Choi, T. W. Noh, H. Zhou, and S. H. Chang. Emergence of robust 2D skyrmions in SrRuO₃ ultrathin film without the capping layer. *Preprint at <https://arxiv.org/abs/1810.01615>*, 2018.
- [35] J. Xia, W. Siemons, G. Koster, M. R. Beasley, and A. Kapitulnik. Critical thickness for itinerant ferromagnetism in ultrathin films of SrRuO₃. *Phys. Rev. B*, 79(14):140407, 2009.
- [36] Y. Ohuchi, J. Matsuno, N. Ogawa, Y. Kozuka, M. Uchida, Y. Tokura, and M. Kawasaki. Electric-field control of anomalous and topological Hall effects in oxide bilayer thin films. *Nat. Commun.*, 9(1):213, 2018.
- [37] S. Onoda, N. Sugimoto, and N. Nagaosa. Intrinsic versus extrinsic anomalous hall effect in ferromagnets. *Phys. Rev. Lett.*, 97:126602, 2006.
- [38] N. Nagaosa, J. Sinova, S. Onoda, A. H. MacDonald, and N. P. Ong. Anomalous Hall effect. *Rev. Mod. Phys.*, 82(2):1539–1592, 2010.
- [39] D. Yue and X. Jin. Towards a better understanding of the anomalous hall effect. *J. Phys. Soc. Jpn.*, 86(1):011006, 2017.
- [40] A. Weiße, G. Wellein, A. Alvermann, and H. Fehske. The kernel polynomial method. *Rev. Mod. Phys.*, 78(1):275, 2006.
- [41] J. H. García, L. Covaci, and T. G. Rappoport. Real-space calculation of the conductivity tensor for disordered topo-

logical matter. *Phys. Rev. Lett.*, 114(11):116602, 2015.

Acknowledgements

We deeply acknowledge fruitful and insightful discussions with Weida Wu, Daniel I. Khomskii, and X. Ren-shaw Wang. This work was supported by the Gordon and Betty Moore Foundations EPiQS initiative through Grant No. GBMF4534. J.H.W. and J.H.P. acknowledge the Aspen Center for Physics where some of this work was completed, which is supported by National Science Foundation grant PHY-1607611.

Author contributions

J.C. and L.W. conceived the original idea. J.C., L.W., F.W., Y.Z., X.L., D.M.V and M.S.K. planned and designed the experiments. F.W., M.K. and L.W. fabricated the samples. L.W., F.W. and J.C. performed transport measurements and data analysis. Y.F., J.H.W. and J.H.P performed numerically exact calculations and the analysis of relevant data. All the authors discussed the results and commented on the manuscript.

Competing interests

The authors declare no competing interests.

Methods

Thin film growth and sample treatment. Ultrathin SRO films were grown on SrTiO₃ (001) substrates using pulsed laser deposition monitored by *in-situ* reflection high-energy electron diffraction (RHEED) (Supplementary Section 1). Prior to the film growth, SrTiO₃(001) substrates were treated to obtain TiO₂-terminated step-and-terrace surfaces [1]. A controlled sequence of time exposure to ambient air treatment was employed to invoke the disorder in the as-grown films.

Transport measurements. Transport measurements for the films were conducted using the d.c. transport option of a physical property measurement system (PPMS, Quantum Design). All the Hall transport data were anti-symmetrized as a function of the magnetic field.

Numerical Calculations. We use the kernel polynomial method to compute the conductivity tensor and the density of states [2]. We average over 100 disorder samples for all of the results presented here.

1. M. Kareev, S. Prosandeev, J. Liu, C. Gan, A. Kareev, J. W. Freeland, M. Xiao, and J. Chakhalian. Atomic control and characterization of surface defect states of TiO₂ terminated SrTiO₃ single crystals. *Appl. Phys. Lett.*, 93(6):061909, 2008.

2. A. Weiße, G. Wellein, A. Alvermann, and H. Fehske. The kernel polynomial method. *Rev. Mod. Phys.*, 78(1):275, 2006.